Modeling, Simulation and Design of Variable Structure Based Sliding Mode Controller for KY-Voltage Boosting Converter

S.SENTAMIL SELVAN[1], K.RAMASH KUMAR[2], R.BENSRAJ[3]

[1]Department of Electrical and Electronic Engineering, SCSVMV University, Taminadu, INDIA
[2]Department of Electrical and Electronic Engineering, Christ Institute of Technology (Formerly by Dr. S.J.S. Paul Memorial College of Engineering and Technology), Puducherry, INDIA
[3]Department of Electrical and Electronic Engineering, Annamallai Unversity, Tamilnadu, INDIA

[1]sentamilselvans@gmail.com; [2]ramash1210@yahoo.co.in; [3]bensraj_au@rediffmail.com

Abstract: – The demand of the non-isolated voltage-boosting converters has experienced an unprecedented augmentation in the last decade. The diversified application domains host the variety of specifications and rating on DC/DC converters and several variations has been addressed, in addition to the basic buck and boost converters. The main issue with them is presence of objectionable level of voltage ripple, which is due the current pulsation. KY series of converters offer solution to this issue and they always dwell in continuous conduction mode (CCM) and imitate the synchronous rectification in performance. This paper presents the analysis, design and load voltage control of positive output KY voltage boosting converter (KY-VBC) using variable structure based sliding mode controller (SMC) for purposes needing the fixed power supply in battery operated portable devices, computer peripheral devices, various medical equipments, industrial and robot system applications etc. The SMC is developed for the innately variable-nature of the KY-VBC with help of the state-space average based model. The performance characteristics of the SMC are verified for its robustness to perform over a wide range of operating conditions through MATLAB/Simulink model in comparison with linear proportional-integral (PI) controller. Theoretical analysis and simulation results are presented along with the complete design procedure.

Key-Words: - DC-DC power conversion, KY-boost converter, sliding mode controller, proportional integral controller, state-space average model.

1 Introduction

The exponential growth in usage of the portable electronic gadgets and other battery operated appliances has added huge research scope to DC-DC converter domain. A good number of DC-DC converter structures have been developed and researched [1]-[5]. The converter structures which are different concept, performance and application suitability and grouped into six generations [6]. The traditional based non-isolated voltage boosting converters namely, boost and buck-boost converters, which produce pulsating load current and they generate objectionable output voltage ripples. In recent days, the conventional DC-DC buck and buck-boost converters with coupling inductors and interleaving control technique has been used to obtain the reduced output voltage ripples of these converters [7]-[9]. However, the appearance of one right-half plane zero (RHPZ) during the continuous conduction mode (CCM) builds it complexity to concomitantly attaining a quick transient load responses. To rectify these issues, the KY-voltage boosting converter (KY-VBC) has been developed [10].

The two types KY-buck-boost converters have been presented [11]. On the other hand, the performance analysis of the designed converter has been studied only in open loop mode. The development of feed-back controllers for switched mode power converters towards various objectives viz. voltage regulation, ripple minimization, power factor correction etc. is well in practice [12]-[13] and still offers a challenging role for design engineers. The fuzzy logic controller (FLC) for KY-VBC has been well presented [14]. But, this controller for the same converter has produced large output voltage ripples and maximum overshoots in start-up transient region. The proportional-integral controller (PIC) for KY-buck-boost converter in

continuous conduction mode (CCM) has been developed [15]-[16]. However, the performance of this converter is validated only at load variations, and also the design of linear PIC parameters has not been presented. Design and implementation of FLC and neuro-fuzzy controller for KY-buck-boost converter/KY-positive boost converter has been reported [17-19]. The results of these controllers have created small overshoots and settling time during line/load variations. In this direction a host of controllers have been suggested for DC-DC power converter [20]-[21]. But, these controllers are very perceptive to converter circuit in parameter variations, different working state, line and load disturbances.

The victory of non-linear controller lies in performing overbearingly against these problems in the variable structure systems (VSS) such as in DC-DC converter [22]. The controller of such system must control with their intrinsic nonlinearity and huge line and load changes, good stability in all operating mode as providing quick transient and superior dynamic responses. Primarily, the sliding mode controller (SMC) applies a large-speed switching control law to drive the non-linear state trajectory onto a precise surface in the state space, called the switching surface, and to maintain it on this surface in the complete process [23]. The SMC recommends many merits over the linear controller. It has an excellent stability during the huge line and load variations, robustness, better dynamic response, and easy implementation. The SMC for Luo-converters has been designed and validated [24]-[26]. The corroboration in these studies proved that the results of SMC in Luo-converter based systems have proficient performance in all operating conditions. The design process as well as performance validation of any system demands an accurate model. The many modeling methods for DC-DC power converters have been addressed [27]-[29]. The state space average model (SSAM) remains most prominent modeling method for DC-DC converters.

The batteries in such applications exhibit provocatively large variations in output voltage, and hence, the robust control is required to operate the switching power supply to regulate the output voltage. The VSS nature of the converter with the battery behavior leaves a challenging task to the controller. The SMC for 2-plus-d KY-VBC has not been addressed still [30]. This paper discusses the modeling, simulation, and design of SMC for 2-plus-d KY-VBC operated in CCM. The dynamic state space equation of same converter is derived at initial and then SMC is developed. The performance of SMC is verified at dissimilar operating states and compared over the linear PI controller.

The organization of paper as follows; Section 2 presents the operation and state space modeling of 2-plus-d KY-VBC. The detailed design of SMC for 2-plus-d KY-VBC is described in section 3. Determination of rating/value of converter circuit elements and its controller parameters are well presented in section 4. Section 5 presents the simulation discussions of 2-puls-d KY-VBC using designed controllers. The conclusions are listed in section 6.

2 Operation and SSAM of Second Order KY-VBC

2.1 Converter Operation

The power circuit of second order-d KY-VBC is depicting in Fig.1 (a) [30]. It consists dc input supply voltage V_{in}, four MOSFET power switches S_{11}, S_{12}, $S_{21,}$ and S_{22} along with their cosspesponding body diodes D_{11}, D_{12}, $D_{21,}$ and D_{22}, energy transferring capacitors C_{E1} and C_{E2}, output inductor L, output capacitor $C_{o,}$ freewheeling diodes D_1 and D_2, output current i_o and load resistance R. The converter is assumed that all the elements are ideal as well as the same converter operates in CCM. Fig.1 (b) and Fig. 1 (c) show the modes of operation of the converter [7].

During state 1 (refer the Fig. 1(b)), the switches, S_{12} and S_{21} are closed and switches, S_{11} and S_{22} are open, the potential across inductor L is equal to V_{in} (across the C_{E1}) plus $2V_{in}$ (across the C_{E2}) and then subtract V_o (the output voltage). The current passing through the C_o is equal to $i_L - i_o$. During state 2 (refer the Fig. 1(c)), the switches, S_{12} and S_{21} are open and switches, S_{11} and S_{22} are closed, the potential across the inductor L is equal to $2V_{in}$ (across the C_{E2}) and then subtract the V_o. The current through the C_o is equal to $i_L - i_o$.

The voltage transfer gain of this converter (by applying the voltage balance to states 1 and 2 operation of the converter) is expressed as follows.

$$G = \frac{V_O}{V_{in}} = 2 + d \tag{1}$$

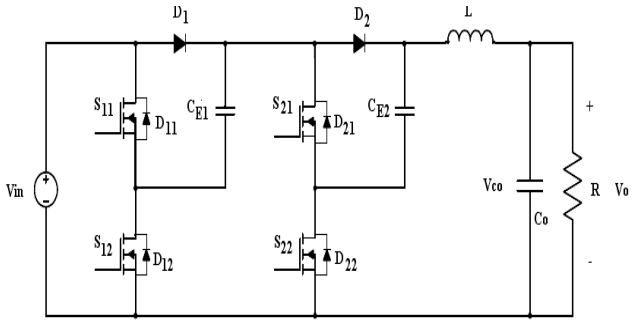

(a)

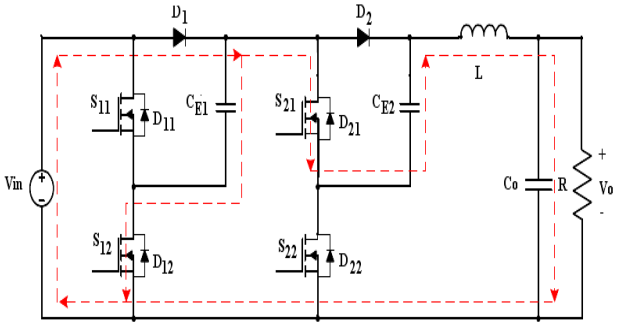

(b)

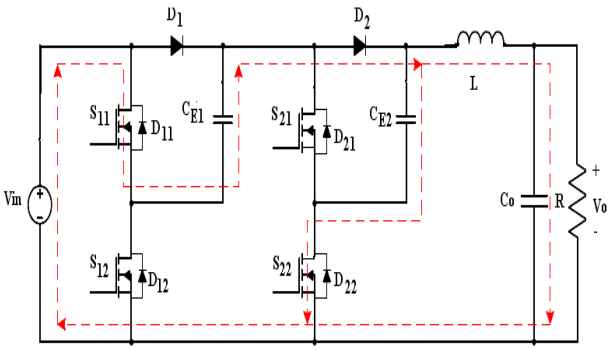

(c)

Fig. 1 Power circuit of second order KY-VBC, (a) topology, (b) equivalent circuit during state 1 operation, and (c) equivalent circuit during state 2 operation.

2.2 SSAM

The state variables of second -order-d KY-VBC are the inductor current, i_L and voltage, V_{Co} respectively taken as x_1 and x_2. During state 1, the dynamic state space equations can be expressed as

$$\begin{cases} \dot{x}_1 = \dfrac{3V_{in}}{L} - \dfrac{V_{Co}}{L} \\ \dot{x}_2 = \dfrac{i_L}{C_o} - \dfrac{V_{Co}}{RC_o} \end{cases} \tag{2}$$

Similarly, state 2, the dynamic state space equation can be written as

$$\begin{cases} \dot{x}_1 = \dfrac{2V_{in}}{L} - \dfrac{V_{Co}}{L} \\ \dot{x}_2 = \dfrac{i_L}{C_o} - \dfrac{V_{Co}}{RC_o} \end{cases} \tag{3}$$

Using the above equations, the complete state-space modeling of the second order KY-VBC with state variables i_{L1}, V_{C1} and V_{C2} can be presented.

$$\begin{bmatrix} \dfrac{di_L}{dt} \\ \dfrac{dV_{Co}}{dt} \end{bmatrix} = \begin{bmatrix} 0 & -\dfrac{1}{L} \\ \dfrac{1}{C_o} & -\dfrac{1}{RC_o} \end{bmatrix} \begin{bmatrix} i_L \\ V_{Co} \end{bmatrix} + \begin{bmatrix} \dfrac{V_{in}}{L} \\ 0 \end{bmatrix} d + \begin{bmatrix} \dfrac{V_{in}}{L} \\ 0 \end{bmatrix} \tag{4}$$

$$\dot{x} = A\,x + B\,d + C \tag{5}$$

Where, d is the status of the switches, x and $\dot{x}$ are the vectors of the state variables (i_L, V_{Co}) and their derivatives respectively.

$$d = \begin{cases} 1 \rightarrow Switches \rightarrow closed \\ 0 \rightarrow Switches \rightarrow open. \end{cases} \tag{6}$$

3 SMC for KY-VBC

3.1 Proposed SMC

The SMC belongs to a class of VSS and being considered for high performance systems. It provides a fast and an accurate response, and makes system response insensitive to changes in the

system parameters, load changes and supply disturbances.

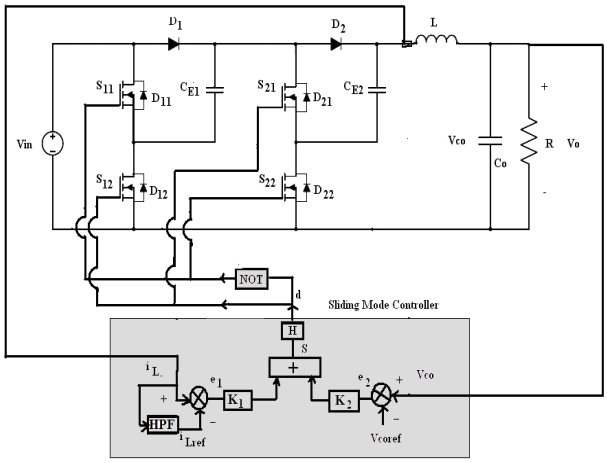

Fig.2. SMC applied to the second order-d KY-VBC

The first step of SMC design is to select a sliding surface that models the desired closed-loop performance in state variable space. Then the control should be designed such that the system state trajectories are forced toward the sliding surface and stay on it. The system state trajectory in the period of time before reaching the sliding surface is called the reaching phase. Once the system trajectory reaches the sliding surface, it stays on it and slides along it to the origin. The system trajectory sliding along the sliding surface to the origin is the sliding mode.

Sensing of all the state variables and the generation of proper references for each of them are the basic needs of a hysteresis modulator (HM) based SMC. According to the principles of a HM based SMC, the capacitor voltage V_{co} are made to follow their references as faithfully as possible, in the voltage loop. On the current loop, the inductor current i_L needs to be tracked with its reference, which depends on the output power demand, the input source voltage and the output voltage. Arriving at the inductor current reference is complicated, because it has to be varied in accordance with load. In case of output voltage regulation, the voltage reference could be a constant (may be arrived from a POT), while setting up of reference for a load dependent current is quite different. This issue can be solved by extracting the inductor current reference, i_{Lref} from the i_L itself by passing it through a high-pass filtering (HPF) under the assumption that their low-frequency component is repeatedly modified as a function of load. Therefore, only the high-frequency component is required for the control. This HPF increases the system order and can seriously affect the converter dynamics. Keeping the cut-off frequency of the HPF as lesser as from the switching frequency can help in improving the dynamics to some extent [27]-[28]. To have a good dynamic characteristic, a sliding surface equation in the state space, which is written by a linear combination of state-variable errors e_i (respective differences of reference current/voltage signals and feedback current/voltage signals), must be chosen optimally.

$$S = (i_L, V_{Co}) = K_1 e_1 + K_2 e_2 \tag{7}$$

Where K_1 and K_2 are sliding surface co-efficients, e_1 is the inductor current error and e_2 is the output capacitor voltage error. The e_1 and e_2 are expressed as below.

$$\begin{aligned} e_1 &= i_L - i_{Lref} \\ e_2 &= V_{Co} - V_{Coref} \end{aligned} \tag{8}$$

By substituting (8) in (7), sliding surface becomes

$$S=(i_L,V_{Co})=K_1(i_L-i_{Lref})+K_2(V_{Co}-V_{Coref}) \tag{9}$$

The sliding surface $S(i_{L,}V_{Co})$ is found by the real time implementation of equation (9) and applied to control circuit (HM). Then, the HM can generate the gate pulses to the MOSFET switches. The complete control model of second order-d KY-VBC is shown in Fig.2. Status of the switch (d) is controlled by hysteresis relay HM, which intends to reduce the error of the variables i_L and V_{Co}. The system response is found by the circuit parameters, and sliding coefficients K_1 and K_2. With a correct choice of these coefficients in any working states, excellent control robustness, stability, and speedy response will be attained.

3.2 Selection of Controller Parameters

In spite of these positive aspects, SMC is not yet popular, probably because it's theoretical complexity and due to the unavailability of straightforward procedure for the selection of controller parameters. In fact, these parameters must be chosen so as to satisfy existence, hitting

and stability conditions [26]. Once the second order KY-VBC input side/output side specifications are selected**,** inductance, L is designed from specified input and output current ripples, capacitors C_o is designed such that the output voltage ripple is limited in the case of fast and large load variations, and maximum switching frequency is selected from the converter ratings and switch type. The system behavior is fully determined by coefficients K_1 and K2, and they must be chosen so as to suit existence, make sure stability and fast response, even for huge supply and load changes. In relation to the VSS theory, the converter equations must be expressed as equation (10) [12].

$$\dot{x} = Ax + Bd + D \tag{10}$$

Where, x represents the vector of state-variables errors and given by

$$\dot{x} = x - X^* \tag{11}$$

Where, $X^* = \left[i_{Lref}, V_{Coref} \right]^T$ is the vector of references.

Substitution of (11) in (2) results the equation (12) [12].

$$D = AX^* + C \tag{12}$$

$$D = \begin{bmatrix} 0 & -\frac{1}{L_1} \\ \frac{1}{C_o} & -\frac{1}{RC_o} \end{bmatrix} \begin{bmatrix} i_{Lref} \\ V_{Coref} \end{bmatrix} + \begin{bmatrix} \frac{V_{in}}{L} \\ o \end{bmatrix} \tag{13a}$$

$$D = \begin{bmatrix} \frac{V_{in}}{L} - \frac{V_{Coref}}{L} \\ \frac{i_{Lref}}{C_o} - \frac{V_{Coref}}{RC_o} \end{bmatrix} \tag{13b}$$

Substituting (11) in (9), the sliding function can be rewritten in the following form.

$$S(x) = K_1 x_1 + K_2 x_2 = K^T x \tag{14}$$

Where $K^T = \left[K_{1,} K_2 \right]$ and $x = \left[x_{1,} x_2 \right]^T$.

The existence condition of the sliding mode requires that all state trajectories near the surface need to be directed towards the sliding plane. The controller can enforce the system state to remain near the sliding plane by proper operation of the converter switch. To make the system state to move towards the switching surface, it is necessary and sufficient that

$$\begin{cases} \dot{S}(x) < 0, if\ S(x) > 0 \\ \dot{S}(x) > 0, if\ S(x) < 0 \end{cases} \tag{15}$$

SMC is obtained by means of the following feedback control strategy, which relates to the status of the switch with the value of S(x):

$$d = \begin{cases} 0, for\ S(x) > 0 \\ 1, for\ S(x) < 0 \end{cases} \tag{16}$$

The existence condition (16) can also expressed as

$$\dot{S}(x) = K^T Ax + K^T D < 0, S(x) > 0 \tag{17}$$

$$\dot{S}(x) = K^T Ax + K^T B + K^T D > 0, S(x) < 0. \tag{18}$$

For the simulation study, by assuming that the error variables x_i are suitably smaller than references X^*, then (17) and (18) can be rewritten as

$$K^T D < 0, S(x) > 0 \tag{19}$$

$$K^T B + K^T D > 0, S(x) < 0. \tag{20}$$

By substituting matrices B and D in (19) and (20), it is engraved as

$$\frac{K_1}{L}\left[V_{in} - V_{coref} \right] + \frac{K_2}{C_o R}\left[Ri_{Lref} - V_{Coref} \right] < 0 \tag{21}$$

$$\frac{K_1}{L}[2V_{in} - V_{coref}] + \frac{K_2}{RC_o}[Ri_{Lref} - V_{coref}] > 0 \tag{22}$$

The existence condition is satisfied if the inequalities (21) and (22) are true. Finally, it is necessary to guarantee that the designed sliding plane is reached for all initial states. If the sliding mode exists, in the system defined by (10), it is a sufficient condition that coefficients, K_1 and K_2 be non-negative.

3.3 Switching Frequency

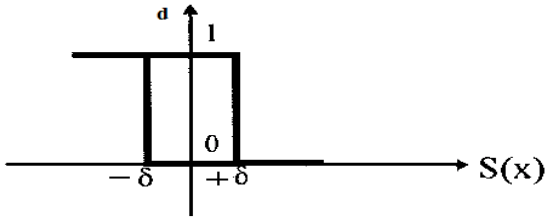

Fig. 3. Switching function d.

In the ideal sliding mode at infinite switching frequency, state trajectories are directed towards the sliding surface and move exactly along it. A practical system cannot switch at infinite frequency. The operating range of the average switching frequency of hysteresis relay varies from 80 kHz to 150 kHz and its corresponding band varies from 0.9 to 0.05. From this operating range, the optimum value of chosen average switching frequency is 100kHz and its corresponding band is 0.5 [13]. A typical control circuit features a practical relay as indicated in Fig. 3. A practical relay always exhibits hysteresis modeled by

.

$$d=\begin{cases}0, & when\ \ S>+\delta\ or\\ & when\,\dot{S}<0 and\,|S|<\delta\\ 1, & when S<-\delta or\\ & when\,\dot{S}>0 and\,|S|<\delta\end{cases} \tag{23}$$

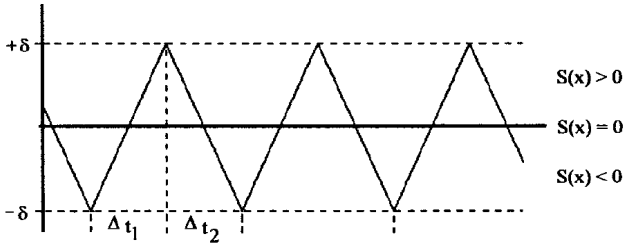

Fig. 4. Phase trajectory slides around the surface with allowed hysteresis band

Where, δ is an arbitrarily small positive quantity and 2δ is the amount of hysteresis in S(x). The hysteresis characteristic makes it impossible to switch the control on the surface S(x) =0. As a consequence, switching occurs on the lines S =±δ, with a frequency depending on the slopes of i_{L1}. This hysteresis causes phase plane trajectory oscillations of width 2δ, around the surface S(x)=0 as shown in Fig. 3. Note that Fig.4 simply confirms that in Δt_1, the function S(x) must increase from –δ to δ for Ś>0, while in Δt_2, it must decrease from +δ to δ for Ś<0. The switching frequency equation is obtained from Fig. 4 by considering that the state trajectory is invariable, near to the sliding surface S(x) = 0.

$$f_s=\frac{1}{\Delta t_1+\Delta t_2} \tag{24}$$

Where, Δt_1 is conduction time of the switches and Δt_2 is the off-time of the switches. The conduction time Δt_1 is derived from (22) and it is given by

$$\Delta t_1=\frac{2\delta}{\frac{K_1}{L}[2V_{in}-V_{coref}]+\frac{K_2}{RC_o}[Ri_{Lref}-V_{coref}]} \tag{25}$$

The off-time Δt_2 is derived from (21), and it is given by

$$\Delta t_2=\frac{-2\delta}{\frac{K_1}{L}\left[V_{in}-V_{coref}\right]+\frac{K_2}{C_oR}\left[Ri_{Lref}-V_{Coref}\right]} \tag{26}$$

The maximum value of switching frequency is obtained substituting (25) and (26) in (24) with the assumption that the converter is operating in no load (i_{Lref} = 0 and 1/R=0) and the output voltage reference is crossing its maximum value ($V_{Coref(max)}$). The maximum switching frequency is obtained as

$$f_{s(\max)}=\frac{K_1V_{in}}{2\delta L}\left(1-\frac{V_{in}}{V_{coref(\max)}}\right) \tag{27}$$

3.4 Duty Cycle

The duty cycle d(t) is defined by the ratio between the conduction time of the switches and the total switching period.

$$d = \frac{\Delta t_1}{\Delta t_1 + \Delta t_2} \quad (28)$$

In view of the SMC, an instantaneous control, the ratio between the output and the input voltages must satisfy the fundamental relation (1) at any working condition.

3.5 Inductor Current

The maximum inductor current ripple is obtained from Fig. 2 and given by [1]

$$\Delta_{iL} = \frac{V_O - V_{in}}{L_1} \Delta_{t1} \quad (29)$$

3.6 Capacitor Voltage

The controller targets to dictate the switches to make the voltage V_{C2} to follow a low-frequency reference. Over $V_{C2}(t)$, a high-frequency ripple (switching) is imposed, which is given as follows [1].

$$\Delta Vco = \frac{V_{Co}}{RC_o} \Delta t_1. \quad (30)$$

It is interesting to note that the switching frequency, inductor current ripple and capacitor voltage ripple depend on control parameters, circuit parameters, reference voltage, output capacitor voltage V_{Co} and inductor current i_L. It is important to determine the circuit parameters and coefficients K_1 and K_2 that agree with desirable values of maximum inductor current ripple, maximum capacitor voltage ripple, optimal switching frequency, stability and fast response for any operating condition.

4 Determination of Circuit Components and Controller Parameters

The main aim of this section is arriving at exact values of various converter elements and controller parameters using previously discussed equations.

4.1Calculation of V_{CO}

Aiming LED TV application, it is decided to have the output voltage as 28V and the corresponding duty cycle of 0.33 is considered for the V_{in} of 12V. The obvious variation of the duty cycle is between the d_{min}= 0.1 and d_{max} = 0.99. Hence the V_{Comax} = 35.88V.

.

4.2 Calculation of Ratio K_1 / L_1

Substituting V_{in}, $V_{Coref\ (max)}$ and δ = 0.5 in (27) the ratio K_1 / L is obtained as 14583.33.

4.3 Calculation of Ratio K_2 /C_O

From (21) and (22), and taking i_{Lref}=$i_{L(max)}$=1.25A (average value), the condition 1608 < K_2 / C_o < 245433 is arrived. There are some degrees of freedom in choosing the ratio K_2/C_o. In this controller, the ratio K_2 / C_o is a tuning parameter. It is recommendable to choose the ratio K_2/C_o to agree with required levels of stability and response speed. The ratio K_2/C_o is chosen by iterative procedure (i.e. the ratio is modified until the transient response is satisfactory), and it is verified by simulation. The final adopted value is K_2/C_o=10000.

4.4 Calculation of L

The maximum inductor current ripple is chosen to be equal to 25 % of maximum inductor current [25], and for this value the L is determined from (29) as 10μH.

4.5 Calculation of Co and values of the coefficients K_1 and K_2

The maximum output capacitor ripple voltage ΔV_{Comax} is chosen to be equal to 0.5 % maximum capacitors voltage [26], and using (30), C_o is calculated as 30μF. Having decided on the values of the ratio K_1/L and inductor, the value of K_1 is unswervingly obtained (K_1 =0.1458). Similarly the

K_2 = 10 is computed using the ratio K_2 / C_o and the C_o.

5 Simulation Study

A detailed simulation study is performed for the designed system in MATLAB/Simulink platform. The final specification used for the study is catalogued in Table 1. The performance of the SMC is obtained first then compared with the typical PI controller. A PI controller with settings K_p = 0.012 and T_i = 0.013s, which are obtained by the Ziegler-Nichols tuning technique is used [21]. The verification of the complete model performance is made for various working states through start-up transient, line variation, load variation, steady state region and in addition circuit elements modifications.

Table 1 Specifications of KY-VBC based system

Parameters	**Symbol**	**Value**
Input Voltage	V_{in}	12V
Output Voltage	V_o	28V
Inductor	L	10µH
Capacitors	C_o , C_{E1}, C_{E2}	1000 µF, 680 µF, 100 µF
Nominal switching frequency	f_s	100kHz
Load resistance	R	15.6Ω
Input Power	P_{in}	56.28W
Output Power	P_o	50.4W
Input Current	I_{in}	4.69A
Output Current	I_o	1.8A
Adopted Value of Duty Ratio	d	0.33
Efficiency		89.9%

5.2 Start-up Region

Fig.5 shows the dynamic response of the output voltage at the start-up for input voltage 12V. It can be seen that output voltage of second order KY-VBC using SMC has a negligible overshoot (M_P) and settling time of 0.01s, whereas the designed PI controller has the settling time (T_s) of 0.04s

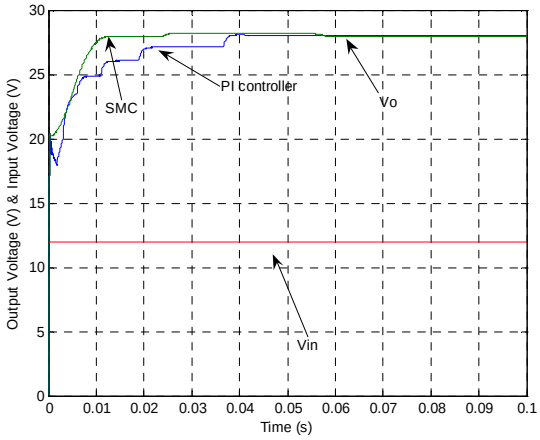

Fig. 5. Response of output voltage of SMC and PI controller in startup for nominal input voltage.

5.2 Line Variations

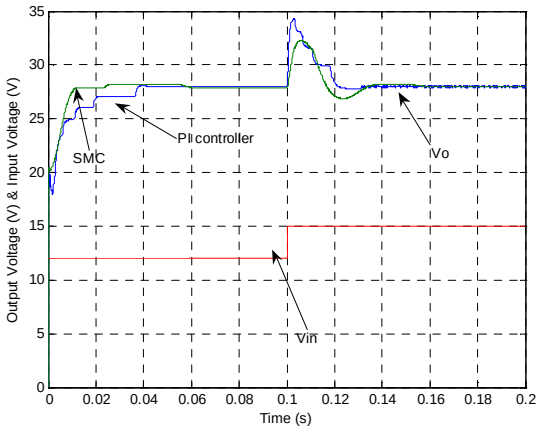

(a)

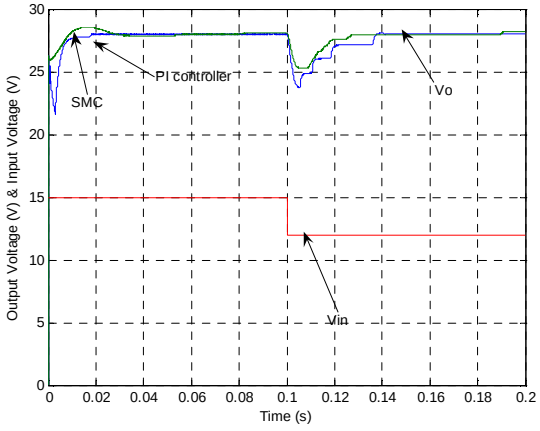

(b)

Fig. 6. The output voltage with rated load, (a) for input step change from 12V to 15 V, (b) for input step change from 15V to 12 V.

Figs.6(a) and 6(b) show the simulation responses of average output voltage using both the PI controller and SMC for input voltage step change from 12V to 15V and 15V to 12V (line variations) at 0.1s respectively. From this figure, it is clearly observed that the simulation responses of output voltage of KY-VBC using SMC has overshoot of 4V and settling time of 0.036 s, while PI controller produces the overshoot as 8V and settling time of 0.02s during the line disturbances.

5.3 Load Variations

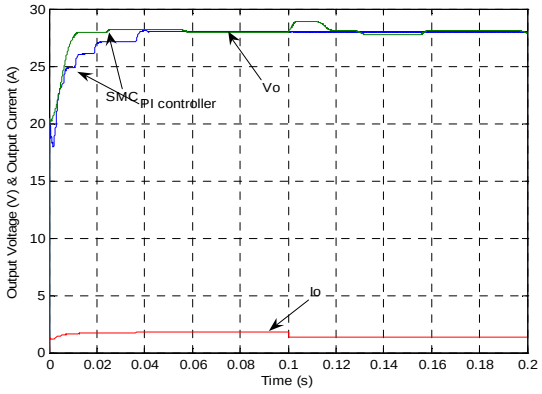

(a)

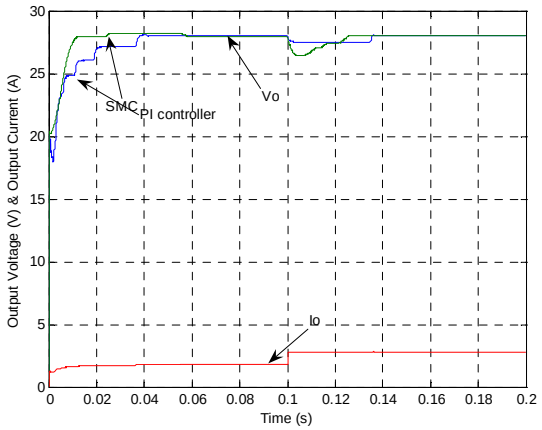

(b)

Fig. 7. The output voltage and current when load value takes a step changes from 15.6Ω to 20Ω and 15.6Ω to 10Ω at time 0.1s with V_{in} = 12V.

Figs. 7 (a) and 7 (b) show the simulation responses of output voltage of KY-VBC using both PI controller and SMC for load step change (15.6Ω to 20Ω and 15.6Ω to 10Ω at time = 0.1s). It could be seen that the simulation results of output voltage of KY-VBC using SMC has a small overshoot of 2V with quick settling time of 0.02s and negligible steady state error, at the same time same model using PI controller has the steady state error of 0.4V.

5.4 Steady State Region

Figs.8(a) and 8(b) show the instantaneous output voltage, output current and the inductor current of KY-VBC in the steady state region using both the SMC and PIC. It is evident from the figure that the output voltage ripple is very small about 0.0001 V (SMC) /0.0006 V (PI controller) and the peak to peak inductor ripple current is 2A for the average switching frequency of 100 kHz closer to theoretical designed value listed in Table 1.

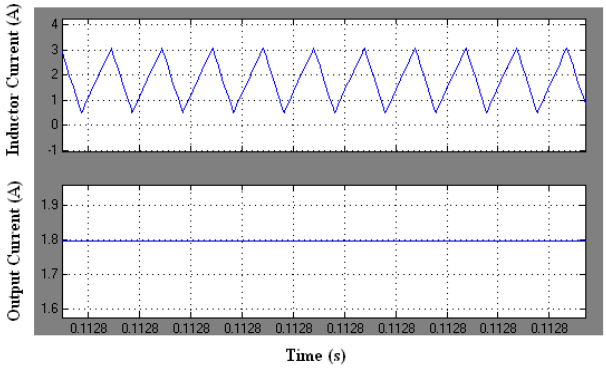

(a)

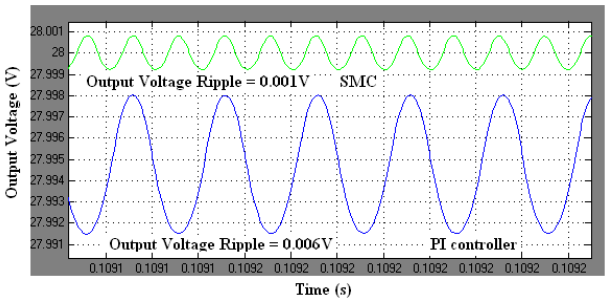

(b)

Fig.8. Response of output voltage and inductor current i_L in steady state condition using both controllers.

Fig. 9 represents the simulation response of output voltage of a KY-VBC using both controllers for inductor L variation from 10µH to 15µH. It could be found that the change does not influence

the KY-VBC behaviors due to proficient SMC than PI controller except little overshoots. An interesting result is illustrated in Fig. 10. It shows the experimental and simulation response of output voltage of a KY-VBC with controllers for the variation in capacitors values from 1000µF to 1500µF. It can be seen that the proposed SMC is very successful in suppressing effect of capacitance variation except that a negligible output voltage ripple and quick settling time with large start-up overshoots.

5.5 Circuit Components Variations

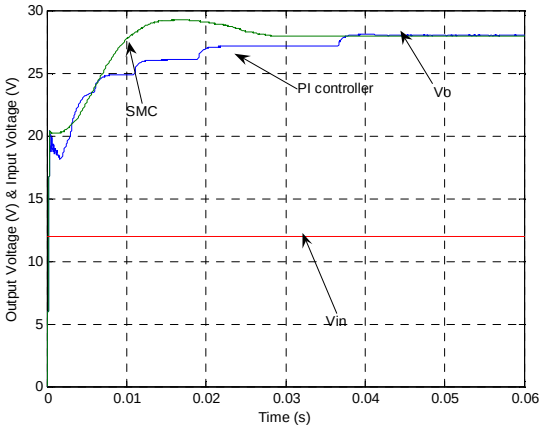

Fig.9. Response of output voltage using SMC and PI controller when inductor variation from 10 µH to 15 µH.

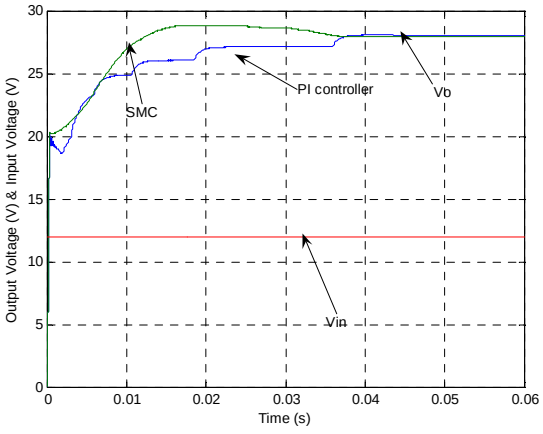

Fig.10. The output voltage using SMC when capacitor variation from 1000µF to 1500µF.

From the Fig.11, it is clearly found that the average input/output currents of the converter with SMC is 4.69A (I_{in})/1.8A (I_o), which are matching with the theoretical designed value given in Table 1. Time domain specifications of KY-VBC using controllers are compared in Table 2. From this table, it is clear that the SMC performance is better in comparison with PI controller.

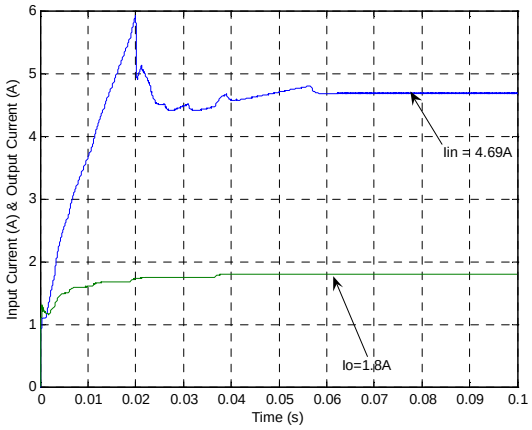

Fig. 11. Response of average input and output currents using SMC.

6 Conclusions

In this paper the analysis, design, and output voltage regulation of second order-d KY-VBC operated in CCM using variable structure based SMC has been successfully demonstrated. The simulation results of SMC has showed that excellent load voltage control, good dynamic responses and reduced output voltage ripple in comparison with linear PI controller. It is, therefore, mainly designed for any fixed power source real-world commercial applications and power supply in battery operated portable devices, medical physiotherapy instrument, mobile phones, lap-tops, personal digital assistant (PDA), MP3 players, blue tooth devices, industrial and LED TV applications etc.

References:

[1] F. L. Luo, Positive output Luo converters: Voltage lift technique, *IEE Proc. Elect. Power Appl.*, Vol. 4, No. 146, Jul. 1999, pp. 415–432.

[2] X. Chen, F. L. Luo, and H. Ye, Modified positive output Luo converter, *in Proc. IEEE Int. Conf. Power Electron. Drive Syst.*, 1999, pp. 450–455.

[3] F. L. Luo and H. Ye, Positive output super-lift converters, *IEEE Trans. Power Electron*., Vol. 18, No. 1, Jan. 2003, pp. 105–113.

[4] F. L. Luo and H. Ye, Positive output multiple-lift push-pull switched capacitor Luo-converters, *IEEE Trans. Ind. Electron*., Vol. 51, No. 3, pp. 594–602, Jun. 2004.

[5] M. J. Johnson, Improvement of stability in current programmed SEPIC DC/DC converters, *in IEEE Applied Power Electronics Conference Proceedings*, 1991, IEEE, March 1991, pp. 452-458.

[6] F.L. Luo F.L and Hong Ye, *Essential DC–DC converters*, New York: CRC Press & Taylor & Francis Group, 2006.

[7] Tseng, C., Liang, T.J, Novel high-efficiency step-up converter, *IEE Proc. Electr. Power Appl*., Vol. 151, 2004, pp.182−190.

[8] Esposito, F., Gentile, G., Isastia, V., Meo S., A, New Bidirectional Soft-Switching Multi-Input DC-DC Converter for Automotive Applications, *International Review of Electrical Engineering (IREE)*, Vol.5, 2010, pp. 1336-1346.

[9] Fang Lin Luo and Hong Ye, *Advanced DC/DC Converters*, (CRC Press, London).

[10] Hwu, K.I., Tu, W.C., and Chen, Y.H., A KY Boost Converter, *IEEE Trans. Power Electronics*, Vol. 25, 2009, pp. 2699 – 2703.

[11] K.I. Hwu, Y.T Yau, Y.T., Two Types of KY Buck–Boost Converters, *IEEE Transactions on Industrial Electronics*, Vol. 56, 2009, pp. 2970 – 2980.

[12] G. Spiazzi and F.C. Lee, Implementation of Single-Phase Boost Power Factor Correction Circuits in Three-Phase Applications, *IEEE Trans. on Industrial Electronics*, Vol. 44, June 1997, pp.365-370.

[13] Salmon, J.C. , Techniques for minimizing the input current distortion of current-controlled single-phase boost rectifiers, *IEEE Trans. Power Electron.*, 1993, Vol. 8, No. 5, pp. 509-520.

[14] Hwu, K.I., Tu, W.C., and Chen, Y.H., On the design of fuzzy-controlled KY converter, *PEDS 2009*, pp. 701 – 705.

[15] Sreedevi, K., David, E., The feedback PI controller for Buck-Boost converter combining KY and Buck converter, *Journal of Academia and Industrial Research (JAIR)*, Vol. 2, 2013, pp. 114-118.

[16] Hwu, K.I., Tu, W.C., and Chen, Y.H., A novel voltage bucking/boosting converter, *PEDS 2009*, pp. 1163 – 1166.

[17] Anand, R., Gnanambal, I., Design and implementation of fuzzy logic controller for KY-buck boost converter, *International review on modeling*, Vol. 7, 2014, pp.221-230.

[18] Karthikumar, S., Mahendran, N., Neuro fuzzy controller for positive output KY boost converter to reduce output voltage ripple, *ELEKTRONIKAIR ELEKTROTECHNIKA*, Vol.19, 2013, pp. 19-24.

[19] Anand, R., Gnanambal, I., Implementation of fuzzy logic controller for buck-boost converter combining KY and Synchronous buck converter for battery operated portable devices, *Journal of Theoretical and Applied Information Technology*, Vol. 67, 2014, pp.151-158.

[20] Forsyth, A.J., Mollow, S.V., Modelling and control of DC–DC converters, *Power Eng. J*., Vol.12, No.5, 1998, pp. 229–236.

[21] Comines, P., Munro, N., PID controllers: recent tuning methods and design to specification, *IEEE Proc. Control Theory Application*, Vol.149, No.1, 2002, pp.46-53.

[22] Utkin, I., *Sliding Mode and Their Application in Variable Structure Systems*, (Moscow, U.S.S.R.: MIR, 1978).

[23] Siw-Chong Tan, Y.M Lai, Chi K.Tse, General Design issues of sliding-mode controllers in DC-DC converters, *IEEE Transactions On Industrial Electronics*, Vol.55, 2008, pp.1160-1174.

[24] Ramash Kumar, K., Jeevananthan, S., Modelling and implementation of fixed switching frequency sliding mode controller for negative output elementary super lift Luo-converter, *IET Power Electron.*, Vol.5, No.8, 2012, pp.1593–1604.

[25] Ramash Kumar, K., Jeevananthan, S., Design of sliding mode control for negative output elementary super lift Luo-Converter operated in continuous conduction mode, *ICCCCT'10*, Tamilnadu, India, pp. 138-148.

[26] Ramash Kumar, K., Jeevananthan, S., Design and implementation of reduced order sliding mode controller plus proportional double integral controller for negative output elementary super lift Luo-Converter, *IET Power Electronics*, Vol.6, No.5, 2013, pp. 974–989.

[27] Middlebrook, R., Cuk, S., A general unified approach to modeling switching-converter power stages, *International Journal of Electronics*, Vol. 42, No. 6, 1977, pp. 521-550.

[28] Mattavelli, P., Rossetto, L., Spiazzi, G., Small signal analysis of DC-DC converter with sliding mode control, *IEEE Transactions on Power Electronics*, Vol. 12, No.1, 1997, pp. 96-102.

[29] F. C. Y. Lee, R. P. Iwens, Y. Yu, and J. E. Triner, Generalized computer-aided discrete time-domain modeling and analysis of dc-dc converters, *IEEE Trans. Ind. Electron. Contr. Instrum*., Vol. 26, May 1979, pp. 58-69.

[30] K. I. Hwu and Y. T. Yau, KY Converter and Its Derivatives, *IEEE Transactions on Power Electronics*, Vol. 24, No.1, 2009, pp.128-137.

Table. 2. Time domain specification analysis of KY-VBC using controllers.

Start up-Region			**Line Variations**				**Load Variations**			
	M_p	**T_s (s)**	**V_{in}=12Vto 15V**		**V_{in}=15Vto 12V**		**R=15.6Ω to 20Ω**		**R=15.6Ω to 10Ω**	
			M_p	**T_s (s)**	**M_p**	**T_s (s)**	**M_p**	**T_s (s)**	**M_p**	**T_s (s)**
SMC	nil	0.012	4V	0.028	2V	0.02	1V	0.008	1V	0.022
PI	nil	0.04	7V	0.022	4V	0.04	nil	nil	0.5V	0.028